Journal of Marine Science and Application (2019) 18:380–386
https://doi.org/10.1007/s11804-019-00102-9

RESEARCH ARTICLE

Feature Extraction for Acoustic Scattering from a Buried Target

Xiukun Li [1,2,3] · Yushuang Wu [1,2,3]

Received: 14 March 2018 / Accepted: 8 November 2018 / Published online: 15 August 2019

Abstract
Elastic acoustic scattering is important for buried target detection and identification. For elastic spherical objects, studies have shown that a series of narrowband energetic arrivals follow the first specular one. However, in practice, the elastic echo is rather weak because of the acoustic absorption, propagation loss, and reverberation, which makes it difficult to extract elastic scattering features, especially for buried targets. To remove the interference and enhance the elastic scattering, the de-chirping method was adopted here to address the target scattering echo when a linear frequency modulation (LFM) signal is transmitted. The parameters of the incident signal were known. With the de-chirping operation, a target echo was transformed into a cluster of narrowband signals, and the elastic components could be extracted with a band-pass filter and then recovered by remodulation. The simulation results indicate the feasibility of the elastic scattering extraction and recovery. The experimental result demonstrates that the interference was removed and the elastic scattering was visibly enhanced after de-chirping, which facilitates the subsequent resonance feature extraction for target classification and recognition.

Keywords Buried target detection · Acoustic scattering · Elastic scattering · De-chirping · Feature extraction

1 Introduction

The detection and recognition of underwater objects buried in the seafloor continue to be a challenge (Chen and Zhou 2012). For a buried target, the common methods can be broadly divided into two categories: imaging detection and non-imaging detection. With imaging sonar (such as synthetic aperture sonar) and image processing, a buried target can be detected and recognized. Studies have shown that the targets and clutter can be sorted according to their acoustic imaging characteristics (Waters et al. 2012b). With localized image symmetry and target strength correlation in 2D feature space, unexploded ordnance (UXO) targets can be separated from at least some non-UXO targets (Bucaro et al. 2008; Bucaro et al. 2012). Compared to imaging detection, non-imaging detection is easier for real-time process, and its requirements on the detection platform are less stringent. In addition, the detection range can be enlarged by transmitting a signal with a lower frequency and smaller grazing angle. Fishell (Fischell and Schmidt 2015) classified seabed spherical and cylindrical targets according to their rigid scattering features. Non-imaging detection implements buried target detection based on its elastic scattering. According to the resonance scattering theory, the scattering from an elastic target contains two terms: background (rigid scattering) and resonance spectrum (elastic scattering) (Junger 1952; Flax et al. 1978). The resonance spectrum reflects the material and internal construction of the target (Gaunaurd and Werby 1991; Morse et al. 1998; Tesei et al. 2002), which are crucial for buried target detection and classification. The elastic contribution to the backscattering from a target remains significant with respect to the specular echo, even when the object is deeply buried (Tesei et al. 2008). The background term has to be removed to obtain the resonance spectrum;

Article Highlights
- For buried target detection and classification, the weak elastic scattering characteristics need to be improved.
- The de-chirping method is adopted here to address the buried target scattering echo.
- The simulation and experimental results are presented and compared with the MIIR result.

✉ Xiukun Li
lixiukun@hrbeu.edu.cn

[1] Acoustic Science and Technology Laboratory, Harbin Engineering University, Harbin 150001, China

[2] Ministry of Industry and Information Technology, Key Laboratory of Marine Information Acquisition and Security (Harbin Engineering University), Harbin 150001, China

[3] College of Underwater Acoustic Engineering, Harbin Engineering University, Harbin 150001, China

however, this is rather difficult in practice because the transmission loss is considerable during wave insonification and propagation in seafloor sediment (Wan et al. 2006). In addition, with an active sonar, the presence of reverberation also impedes target detection. There are two popular methods for elastic scattering extraction, namely time inverse technology and the method of isolation and identification of resonance (MIIR). The time inverse technology for buried target detection was introduced by Waters (Waters et al. 2009). The procedure consists of exciting the target object with a broadband pulse, sampling the return with a finite time window, reversing the signal in time, and using this reversed signal as the source waveform for the next interrogation. It has been indicated that the spectrum of the returns rapidly converges to the dominant mode in the backscattering response, and the signal-to-noise of the target echo is enhanced for a target buried in different depths (Waters et al. 2012a; Waters and Barbone 2012; Yu et al. 2014). The MIIR, which was introduced by G. Maze (Maze et al. 1988; Maze et al. 1989), extracts elastic scattering in the time domain by transmitting a narrow pulse. Experimental results have shown that the resonance spectrum is visible with the MIIR, and it is effective for buried target detection (Maze 1991; Décultot et al. 2010).

It is well known that resonance characteristics are significant for target classification; however, the elastic scattering needs to be enhanced as it is usually disturbed by the propagation loss and the interference of reverberation. In this study, to remove the reverberation and specular echo and highlight the elastic resonant characteristics, de-chirping method (Caputi 1971) was adopted when a linear frequency modulation (LFM) signal was transmitted. An echo could be transformed into a series of signals with different frequencies, and the elastic ones could be filtered out with a band-pass filter and then recovered by remodulation. The experimental result shows that the resonance was visibly enhanced after processing, which is beneficial to the next resonance feature extraction for target classification and recognition.

2 Simulation and Analysis of Buried Target Scattering

The target in this study was a stainless steel sphere with a radius of 0.079 cm, which was buried in the sand-water mixture at a depth of 2 cm. Table 1 lists the selected physical properties for the

Table 1 Material parameters

Material	Longitudinal wave speed c_p (m/s)	Transverse wave speed c_p (m/s)	Density ρ (kg/m^3)
Water	1500	0	1000
Sand	1600	0	1800
Stainless steel	5940	3100	7900

numerical simulations. A COMSOL model (Hu et al. 2016) was built to obtain the theoretical scattering of the target. Considering the limitation of hardware, the calculation frequency range was set from 60 to 120 kHz with an interval of 100 Hz. The frequency response is shown in Fig. 1. The blue line is the normal series solution of the free-field scattering with a frequency interval of 5 Hz, and the red one is the COMSOL result of the buried target when the attenuation coefficient of sand was 0.5 dB/λ.

Compared to the normal series result of the target in free field, there was no marked change in the frequency response of that in the buried condition, except a slight intensity decrease due to the absorption of sand. A Hanning window was used as a band-pass filter, and the waveform of the inverse Fourier transformation (Anderson et al. 2012) is shown in Fig. 2, where the left one is the waveform of the free-field scattering, and the right one is that of the buried target. For both free-field and buried target scattering, series of narrowband energetic arrivals follow the first specular one, i.e., elastic echo, while their amplitudes rapidly drop over time. Then, the MIIR was employed, and the specular and the elastic scattering were separated in the time domain, the spectra of which are shown in Fig. 3. In the figure, the upper panel gives the result of free-field scattering, where the left is the spectrum of the specular echo, and the right is that of the elastic ones; similarly, the bottom panel is the result of the buried situation. For free-field scattering, the specular echo spectrum was consistent with the incident signal, while there were more details of elastic scattering after the MIIR. The same results were obtained for the buried situation.

The above analysis was performed without considering the incident signal, which is important for signal processing. In underwater studies, LFM signals are very popular because of their pulse compression. Suppose the frequency modulation range of the transmitted LFM signal was from 60 to 120 kHz, and the pulse width was 100 sampling points; the corresponding waveform and elastic spectrum are shown in Fig. 4. The

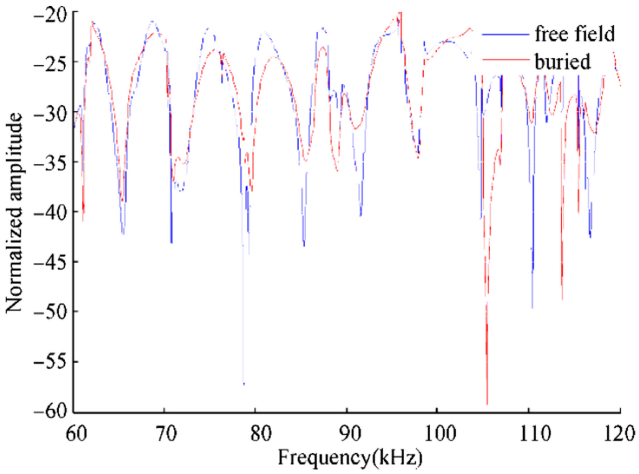

Fig. 1 Simulation of the scattering from a sphere in free field and in a buried condition

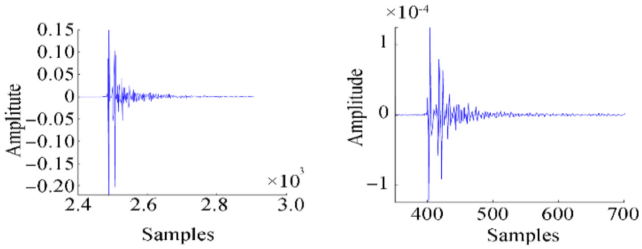

(a) Free-field target scattering waveform (b) Buried target scattering waveform

Fig. 2 Waveform of free-field and buried target scattering, **a** free-field target scattering waveform, **b** buried target scattering waveform

aliasing of the rigid scattering and the elastic ones is expected to be noticed when we increase the pulse width of the incident signal. Figure 5 presents the scattering waveforms when the pulse widths were 1000 and 2000 sampling points. With a larger pulse width, the specular echo and elastic scattering were mixed in the time domain. In this situation, it was not easy to extract the exact elastic echo in the time domain with the MIIR; thus, the de-chirping method was employed.

3 De-chirping Processing

In engineering, a target can be considered as a linear time-invariant system and the target echo as the system response to the incident signal. In the far field, according to the highlight model (Tang 1994), a target echo can be written as the superposition of a series of subwaves, i.e., highlights. The

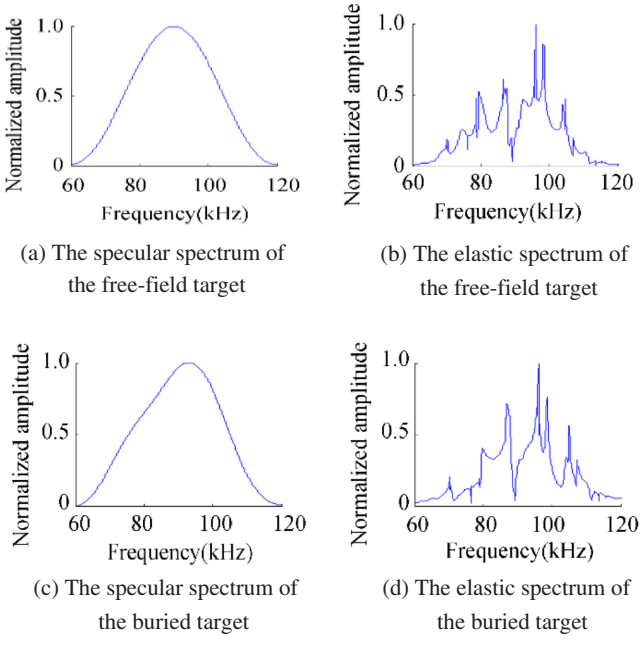

(a) The specular spectrum of the free-field target (b) The elastic spectrum of the free-field target

(c) The specular spectrum of the buried target (d) The elastic spectrum of the buried target

Fig. 3 Spectra of the specular and elastic echo for a free-field (upper panel) and buried (under panel) sphere. **a** The specular spectrum of the free-field target. **b** The elastic spectrum of the free-field target. **c** The specular spectrum of the buried target. **d** The elastic spectrum of the buried target

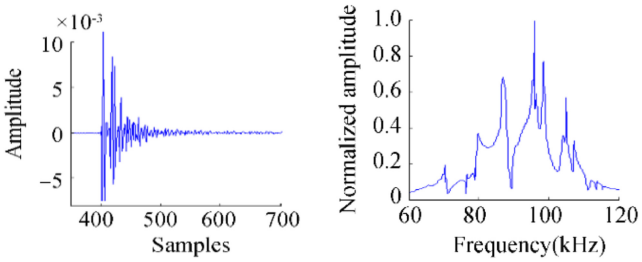

(a) The wave form (b) The elastic echo spectrum

Fig. 4 Waveform and elastic echo spectrum of the buried target when the pulse width of incident LFM signal was 100 sampling points. **a** The waveform, **b** the elastic echo spectrum

frequency modulation properties of specular echo and elastic scattering are basically the same (Li et al. 2015), although they have different frequency responses. To simplify the analysis, every highlight is considered as a time-delay copy of the incident signal, without considering the amplitude response and phase jump.

An incident LFM signal can be written as

$$s(t) = \exp\left[j2\pi\left(f_0 t + 0.5kt^2\right)\right] \tag{1}$$

where $k = (f_1 - f_0)/T$ is the slope of frequency modulation, $f_0 \sim f_1$ is the frequency range, and T is the pulse width.

A single scattering component can be described as

$$x_i(t) = \exp\left[j2\pi f_0(t-\tau_i) + j\pi k(t-\tau_i)^2\right], \tag{2}$$

where τ_i is the corresponding time delay.

An LFM signal with a fixed time and the same frequency and frequency modulation are taken to execute a conjugate convolution with the signal to be processed. Select a reference point between the target and receiver, which is R_{ref} away from the receiver, then the time delay is $\tau_{\text{ref}} = 2R_{\text{ref}}/c$, where c is the sound speed. The reference signal is

$$s_{\text{ref}}(t) = \exp\left[j2\pi f_0(t-\tau_{\text{ref}}) + j\pi k(t-\tau_{\text{ref}})^2\right] \tag{3}$$

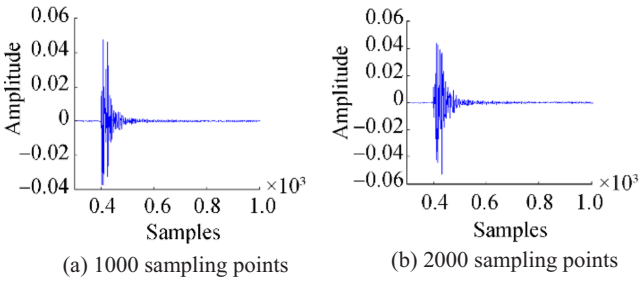

(a) 1000 sampling points (b) 2000 sampling points

Fig. 5 Waveform of the buried target when the pulse widths of incident LFM signal were 1000 and 2000 sampling points, **a** 1000 sampling points, **b** 2000 sampling points

Multiply Eq. (3) with the conjugate of Eq. (2) and we will get

$$y_i(t) = \exp[j2\pi(kt + f_0)(\tau_i - \tau_{ref})] \exp\left[j\pi k\left(\tau_{ref}^2 - \tau_i^2\right)\right] \quad (4)$$

which can be seen as a single-frequency signal, and the frequency is proportional to the time delay (Xia and Li 2015). If $\tau_{ref} = 0$, then Eq. (4) can be rewritten as.

$$y_i(t) = \exp[j2\pi k\tau_i t] \exp\left[j2p\left(f_0\tau_i\tau 0.5k\tau_i^2\right)\right]. \quad (5)$$

This way, scattering with different time delays from a buried target can be seen as a series of single-frequency signals with different frequencies. Therefore, through a band-pass filter, the elastic components of the target scattering can be extracted, and the rigid scattering and interference can be removed. The procedure consists of the following steps:

1) De-chirping the observed signal: With the known parameters of the incident signal, the scattering signal is de-chirped as mentioned above.
2) Band-pass filtering the de-chirped signal: The elastic components are filtered out by several band-pass filters, and the center frequencies of the filters are determined based on the peak frequencies of the de-chirped signal.
3) Recovering the filtered component: The elastic scattering components are recovered by remodulating the filtered signal with the transmitted signal.

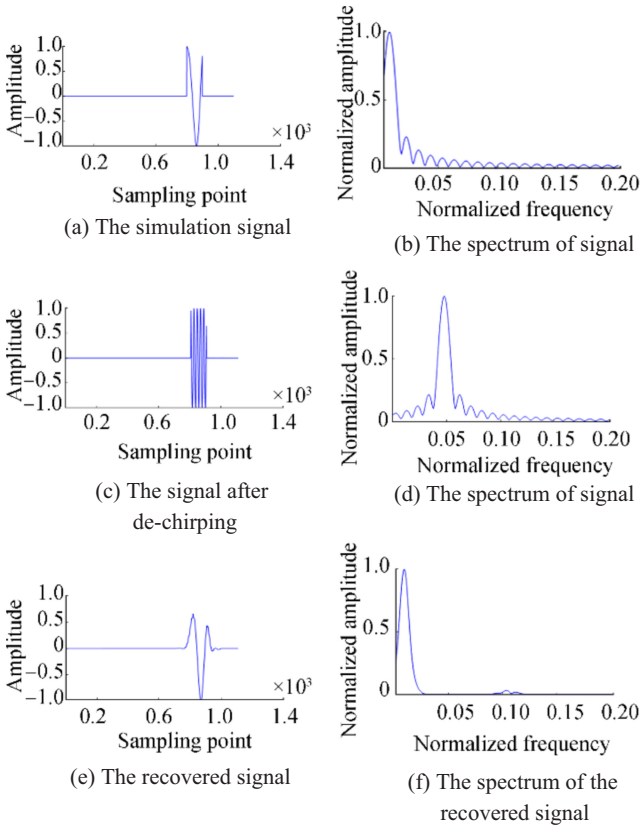

Fig. 6 Simulation of de-chirping

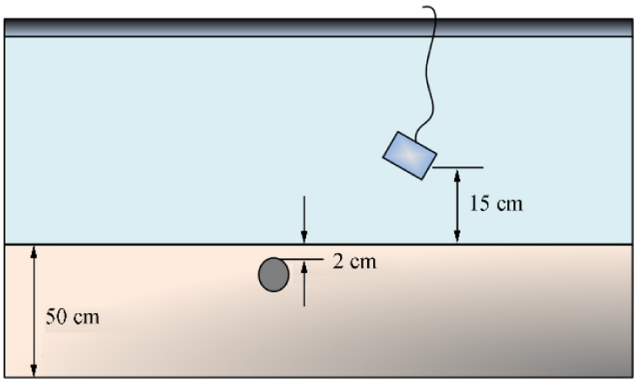

Fig. 7 Diagram of the experiment setup

To verify the proposed method, we consider an LFM signal whose frequency range was 60 to 120 kHz and pulse width was 100 sampling points, and the result of de-chirping is shown in Fig. 6. Figures 6 (a) and (b) are the waveform and spectrum of the simulated signal, respectively. Figures 6 (c) and (d) are the waveform and spectrum of the signal after the de-chirping process. Figures 6 (e) and (f) are the waveform and spectrum of the recovered signal. The correlation

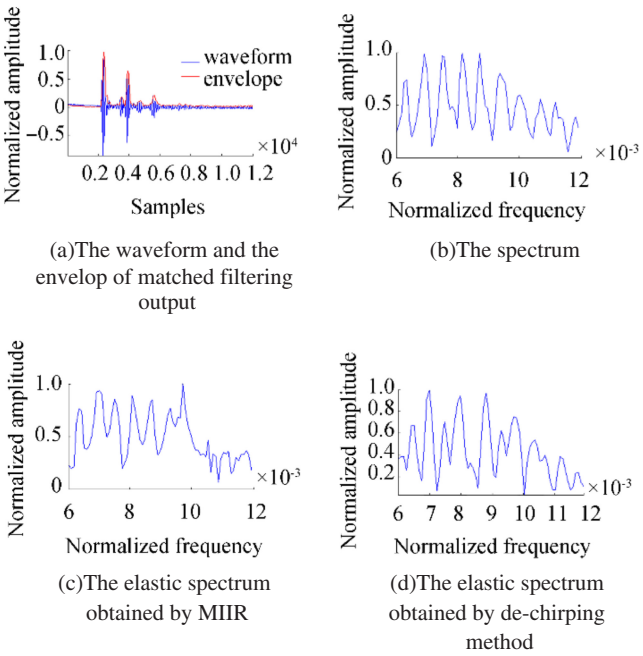

Fig. 8 The results when the pulse width of the transmitted signal was 100 sampling points, **a** the waveform and the envelop of matched filtering output, **b** the spectrum, **c** the elastic spectrum obtained by MIIR, and **d** the elastic spectrum obtained by the de-chirping method

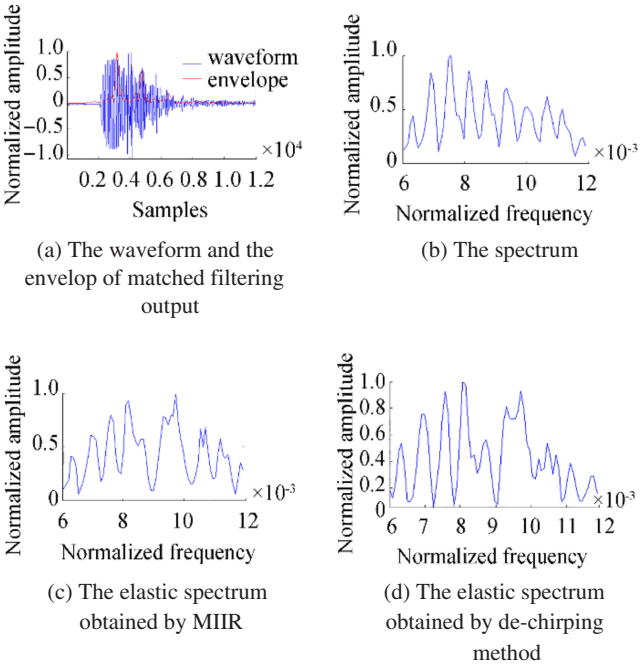

(a) The waveform and the envelop of matched filtering output

(b) The spectrum

(c) The elastic spectrum obtained by MIIR

(d) The elastic spectrum obtained by de-chirping method

Fig. 9 The results when the pulse width of the transmitted signal was 2000 sampling points, **a** the waveform and the envelop of matched filtering output, **b** the spectrum, **c** the elastic spectrum obtained by MIIR, **d** the elastic spectrum obtained by the de-chirping method

coefficients of the signals (Figs. 6 (a) and (e)) and their spectra (Figs. 6 (b) and (f)) are 0.9183 and 0.9650, respectively. This indicates that de-chirping method is suitable for elastic scattering extraction.

4 Experimental Signal Processing

To further verify the effectiveness of the de-chirping method, an experimental signal was processed. The experiment was conducted in a pool at Shanghai Jiaotong University, and the experimental setup and the parameters are shown in Fig. 7 (Hu et al. 2016). A stainless steel sphere was buried in sand at a depth of 2 cm. The transmitter and receiver were joined into a monostatic device, which could move horizontally through the guide rail above the target.

Before burying the sphere in the sand-water mixture, the backscattering in the free field was collected. The signal mentioned in Section 3 was transmitted, and the scattering echo is shown in Fig. 8. Figure 8(a) is the waveform of the backscattering echo and the envelope after matched filtering. As the object was suspended in the pool with a rope, the second arrival was the scattering of the rope. Figure 8(b) is the spectrum, (c) is the elastic scattering obtained by the MIIR, including the rope scattering, and (d) is the pure elastic scattering obtained by the de-chirping method. The resonance peaks in the spectrum of the entire echo are very close to the theoretical result shown in Fig. 1.

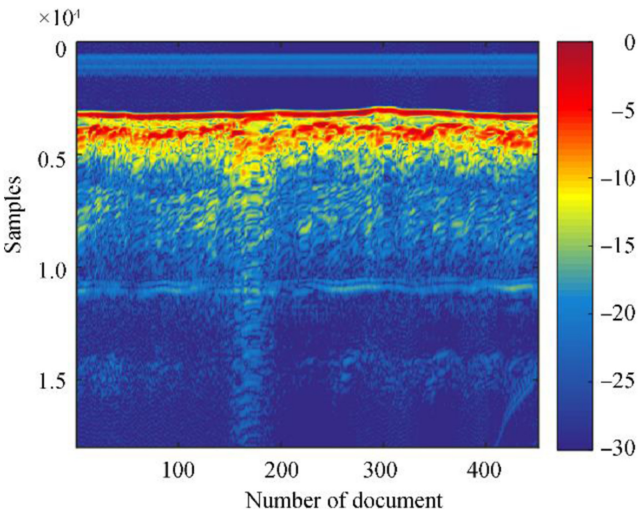

Fig. 10 Result of the matched filter

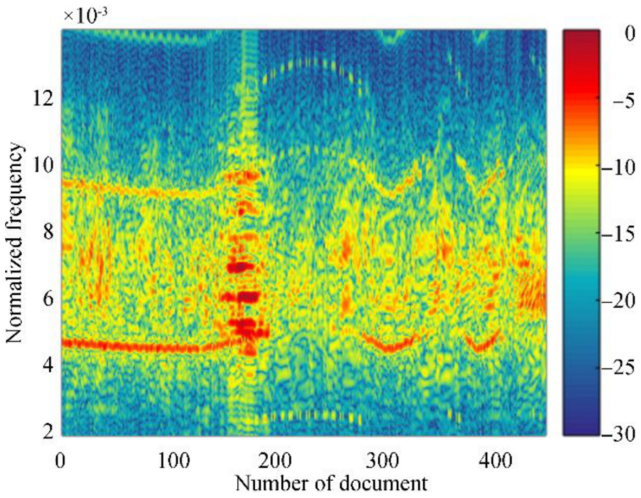

Fig. 11 The MIIR result

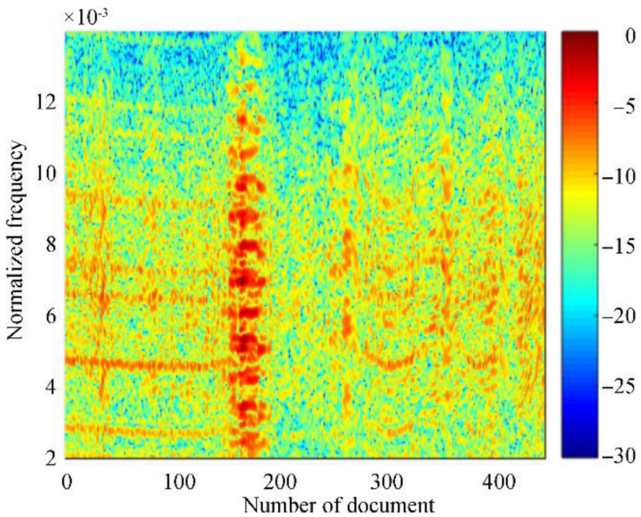

Fig. 12 The de-chirping method result

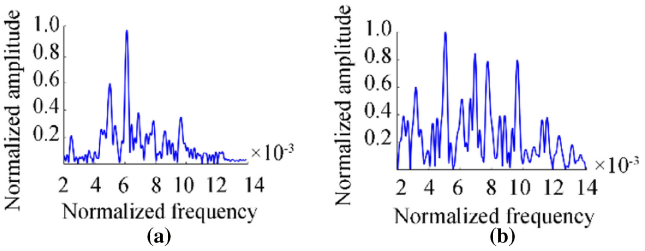

Fig. 13 Comparison of the MIIR and de-chirping results in the buried condition

Compared with the MIIR, the de-chirping method could obtain the pure elastic scattering from the sphere with no interference from the rope, and it could improve the scattering in the high frequency.

Similar results were obtained when the pulse width of the transmitted signal was 2000 sampling points (Fig. 9). The specular echo and the elastic echo were mixed together in the time domain, and it was difficult to obtain the pure elastic scattering echo. The de-chirping method yielded more details and accurate information.

The same signal whose pulse width was 100 sampling points was transmitted for the buried object, and the recorded echo of 75° grazing angle was processed. From the result of the matched filter, shown in Fig. 10, it is difficult to locate the target only with the specular scattering; however, there is a long trailing around the 170th document, which is where the target might be. To confirm this, the MIIR was applied, and the result is shown in Fig. 11. There are several resonance peaks at the suspected position of the target. Notwithstanding, the signal needs to be improved to facilitate the following resonance feature extraction, which is significant for target classification and recognition. The signal was processed using the de-chirping method, and the result is shown in Fig. 12. In contrast to the MIIR result, the number of resonance peaks increased, which means some weak elastic components were extracted and enhanced. Figure 13 shows the specific results of the MIIR and the de-chirping method for the 170th document. With the de-chirping method, some resonance peaks were enhanced despite that one of them was depressed. This proves that the elastic scattering can be extracted and enhanced with the proposed method, which will benefit the buried target classification and recognition.

5 Conclusion

According to the result of the COMSOL simulation, the scattering of a buried sphere was consistent with the scattering when it was in free field. With a narrow bandwidth pulse, a series of narrowband energetic arrivals were observed to follow the specular arrival. However, for the propagation loss and the interference of reverberation, the elastic components which are significant for target detection and classification, were difficult to obtain. To extract and enhance the elastic scattering, the de-chirping method was adopted to address the buried target scattering. The experimental result demonstrates that with the de-chirping process, the elastic components could be improved compared with the MIIR result, and it was beneficial to the subsequent resonance feature extraction, which was crucial to the target classification and recognition.

References

Anderson SD, Sabra KG, Zakharia ME, Sessarego JP (2012) Time-frequency analysis of the bistatic acoustic scattering from a spherical elastic shell. J Acoust Soc Am 131(1):164–173. https://doi.org/10.1121/1.3669995

Bucaro JA, Houston BH, Saniga M, Dragonette LR, Yoder T, Dey S, Kraus L, Carin L (2008) Broadband acoustic scattering measurements of underwater unexploded ordnance (UXO). J Acoust Soc Am 123(2):738–746. https://doi.org/10.1121/1.2821794

Bucaro JA, Waters ZJ, Houston BH, Simpson HJ, Sarkissian A, Dey S, Yoder TJ (2012) Acoustic identification of buried underwater unexploded ordnance using a numerically trained classifier (L). J Acoust Soc Am 132(6):3614–3617. https://doi.org/10.1121/1.4763997

Caputi WJ (1971) Stretch: a time-transformation technique. IEEE Trans Aerosp Electron Syst 7(2):269–278. https://doi.org/10.1109/TAES.1971.310366

Chen XP, Zhou LS (2012) Review of current status of buried-object detection techniques. Tech Acoust 31(1):30–35 (in Chinese). https://doi.org/10.3969/j.issn1000-3630.2012.01.004

Décultot D, Liétard R, Maze G (2010) Classification of a cylindrical target buried in a thin sand-water mixture using acoustic spectra. J Acoust Soc Am 127(3):1328–1334. https://doi.org/10.1121/1.3298430

Fischell EM, Schmidt H (2015) Classification of underwater targets from autonomous underwater vehicle sampled bistatic acoustic scattered fields. J Acoust Soc Am 138(6):3773–3784. https://doi.org/10.1121/1.4938017

Flax L, Dragonette LR, Überall H (1978) Theory of elastic resonance excitation by sound scattering. J Acoust Soc Am 63(3):723–731. https://doi.org/10.1121/1.381780

Gaunaurd GC, Werby MF (1991) Sound scattering by resonantly excited, fluid-loaded, elastic spherical shells. J Acoust Soc Am 90(5):2536–2550. https://doi.org/10.1121/1.402059

Hu Z, Fan J, Zhang PZ, Wu YS (2016) Acoustic scattering from elastic target buried in water-sand sediment. Acta Phys Sin 65(6):064301 (in Chinese). https://doi.org/10.7498/aps.65.064301

Junger MC (1952) Sound scattering by thin elastic shells. J Acoust Soc Am 24(4):366–373. https://doi.org/10.1121/1.1906905

Li XK, Meng XX, Xia Z (2015) Characteristics of the geometrical scattering waves from underwater target in fractional Fourier transform

domain. Acta Phys Sin 64(6):64302 (in Chinese). https://doi.org/10.7498/aps.64.064302

Maze G (1991) Acoustic scattering from submerged cylinders. MIIR Im/re: experimental and theoretical study. J Acoust Soc Am 89(6):2559–2566. https://doi.org/10.1121/1.400684

Maze G, Lecroq F, Izbicki JL, Ripoche J (1988) Acoustic resonance spectra of a finite cylindrical shell. J Acoust Soc Am 83(S1):S95. https://doi.org/10.1121/1.2025604

Maze G, Lecroq F, Izbicki JL, Ripoche J, Numrich S (1989) Acoustic scattering from an air-filled prolate cylinder. J Acoust Soc Am 85:S94–S94. https://doi.org/10.1121/1.2027222

Morse SF, Marston PL, Kaduchak G (1998) High-frequency backscattering enhancements by thick finite cylindrical shells in water at oblique incidence: experiments, interpretation, and calculations. J Acoust Soc Am 103(2):785–794. https://doi.org/10.1121/1.421200

Tang WL (1994) Highlight model of echoes from sonar targets. Acta Acust 19(2):93–100 (in Chinese). https://doi.org/10.15949/j.cnki.0371-0025.1994.02.002

Tesei A, Maguer A, Fox WL, Lim R, Schmidt H (2002) Measurements and modeling of acoustic scattering from partially and completely buried spherical shells. J Acoust Soc Am 112(5 Pt 1):1817–1830. https://doi.org/10.1121/1.1509425

Tesei A, Fawcett JA, Lim R (2008) Physics-based detection of man-made elastic objects buried in high-density-clutter areas of saturated sediments. Appl Acoust 69(5):422–437. https://doi.org/10.1016/j.apacoust.2007.04.002

Wan L, Fan J, Tang WL (2006) The target strength and echo-to-reverberation ratio of a buried target in sediment. Acta Acust 31(2):151–157 (in Chinese). https://doi.org/10.3321/j.issn:0371-0025.2006.02.010

Waters ZJ, Barbone PE (2012) Discriminating resonant targets from clutter using Lanczos iterated single-channel time reversal. J Acoust Soc Am 131(6):EL468–EL474. https://doi.org/10.1121/1.4718592

Waters ZJ, Dzikowicz BR, Holt RG, Roy RA (2009) Sensing a buried resonant object by single-channel time reversal. IEEE Trans Ultrason Ferroelectr Freq Control 56(7):1429–1441. https://doi.org/10.1109/TUFFC.2009.1198

Waters ZJ, Dzikowicz BR, Simpson HJ (2012a) Isolating scattering resonances of an air-filled spherical shell using iterative, single-channel time reversal. J Acoust Soc Am 131(1):318–326. https://doi.org/10.1121/1.3669971

Waters ZJ, Simpson HJ, Sarkissian A, Dey S, Houston BH, Bucaro JA, Yoder TJ (2012b) Bistatic, above-critical angle scattering measurements of fully buried unexploded ordnance (UXO) and clutter. J Acoust Soc Am 132(5):3076–3085. https://doi.org/10.1121/1.4757098

Xia Z, Li XK (2015) Separation of elastic acoustic scattering of underwater target. Acta Phys Sin 64(9):094302 (in Chinese). https://doi.org/10.7498/aps.64.094302

Yu XT, Peng LH, Yu GK (2014) Extracting the subsonic anti-symmetric lamb wave from a submerged thin spherical shell backscattering through iterative time reversal. J Ocean Univ China 13(4):589–596. https://doi.org/10.1007/s11802-014-2166-8